



Adsorptive removal of As(V) by crawfish shell biochar: batch and column tests

Jinpeng Yan¹ · Yingwen Xue¹ · Li Long¹ · Yifan Zeng¹ · Xiaolan Hu¹

Received: 3 July 2018 / Accepted: 1 October 2018 / Published online: 15 October 2018
© Springer-Verlag GmbH Germany, part of Springer Nature 2018

Abstract

As a toxic and metalloid substance, excess arsenic (As) can cause serious harm to the environment and public health. In this work, crayfish shell biochar (CFS450) and modified biochar (MCFS450) were prepared to remove As(V) from aqueous solutions under various conditions. Compared to CFS450, MCFS450 had a higher specific surface area, better pore structure, and higher As(V) adsorption capacity. Based on the Langmuir model, its maximum As(V) adsorption capacity was 17.2 mg/g. The biochar had a large number of surface functional groups such as C-O, O-H, and -OH. After modification, a certain mass of ZnO nanoparticles existed on MCFS450, which increased positive charge on the surface and promoted the adsorption of As(V). As the temperature rose, the adsorption capacity increased, suggesting the adsorption was endothermic. Under low PH conditions, the adsorption effect was better. When Cl^- , HCO_3^- , SO_4^{2-} , and PO_4^{3-} respectively existed, the adsorption capacity decreased, indicating that As(V) competed with other anions. The column adsorption experiments showed that Thomas, Yoon-Nelson, and Adams-Bohart models can be expressed as a unified model (EXY model). The EXY model can be used for the design of biochar-based filter for As(V) removal, providing a theoretical basis for practical production applications.

Keywords Crawfish shell biochar · ZnO nanoparticles · Column adsorption · Adsorption model

Introduction

Arsenic in the aqueous environment often exists in the inorganic forms, such as As(III) and As(V) (Naito et al. 2015). It is proved that arsenic-containing compounds can cause great harm to human health (Egodawatta et al. 2018). Exposure to arsenic-containing environment can contribute to chronic arsenic poisoning and many serious diseases (Liu et al. 2015). Therefore, finding an efficient and rapid arsenic removal

method has become one of the hot topics in the field of water treatment.

Numerous techniques have been applied to remove arsenic from aqueous solutions, such as adsorption, oxidation, precipitation, ion exchange, adsorption, reverse osmosis, and membrane separation. Among these methods, adsorption has the advantages of simple operation process, large treatment capacity, and fast adsorbing speed (Li et al. 2010). Biochar has been widely used to remove arsenic because of its large surface area, high total pore volume, and excellent chemical stability. For example, Zhang et al. (2015) used sludge-derived biochar to remove As(III) and found its adsorption capacity of 3.08–6.04 mg/g. At the same time, using suitable substances to modify biochar can improve its adsorption capacity to arsenic. Xia et al. (2016) used ZnCl_2 as a modifier and the resultant ZnCl_2 -activated biochar had a maximum As(V) adsorption capacity of 27.67 mg/g. Jin et al. (2014) found that the highest adsorption capacity of a biochar produced from municipal solid wastes for As(V) was 24.49 mg/g. After being activated by 2.0 M KOH solution, its adsorption capacity increased to 30.98 mg/g.

However, the above studies did not conduct the column experiments. Continuous flow processes such as fixed bed

Highlights

- After modification, MCFS450 possessed ZnO nanoparticles.
- Thomas, Yoon-Nelson, and Adams-Bohart models can be expressed as a unified equation (EXY model).
- The performance of continuous adsorption columns could be predicted by the EXY model ($R^2 = 0.97\text{--}0.99$).

Responsible editor: Tito Roberto Cadaval Jr

✉ Yingwen Xue
ywxue@whu.edu.cn

¹ School of Civil Engineering, Wuhan University, Wuhan, China

column experiment are meaningful because of their practical engineering values. Mathematical models including Thomas, Yoon-Nelson, and Adams-Bohart models are commonly used to describe the continuous flow processes, and the Thomas model is the most frequently used. Colak et al. (2013) used Thomas model to describe the column data and found Thomas model ($R^2 = 0.982\text{--}0.992$) has a perfect fit for the breakthrough curve. Jaiswal et al. (2018) used four novel fungal strains to remove arsenic and found a high correlation (ranging from $R^2 = 0.940\text{--}0.972$) between experimental and predicted value using Thomas model. Based on experimental data, Atar et al. (2011) concluded that Thomas model is suitable for adsorption processes where external and internal diffusion limitations are absent. Although there are many investigations on continuous flow processes, only few have compared the Thomas, Yoon-Nelson, and Adams-Bohart models and studied their possible intrinsic links.

In this work, Thomas, crayfish shell was selected as the feedstock because of its wide range of sources and excellent chemical stability. Biochar (CFS450) was converted from crayfish shell at 450 °C. Modified biochar (MCFS450) was made with ZnCl_2 (3 M) as a modifier. Laboratory batch and column sorption experiments were used to determine the effect of biochar on the removal of As(V). In addition, Thomas, Yoon-Nelson, and Adams-Bohart models were used to describe the continuous flow processes. The main objective of this work is to evaluate the application of biochar derived from crayfish shell in the treatment of arsenic contaminated water.

Materials and methods

Materials

In this experiment, crayfish shell was used as the feedstock. All the chemical reagents were at analytical grades. Deionized water was used to prepare chemical solutions.

Biochar production

Certain mass of crayfish shell was heated in a high-temperature quartz glass tube filled with N_2 at the temperature of 450 °C for 2 h (Gao et al. 2015; Xu et al. 2015). Then, the glass tube was cooled to room temperature and the crayfish shell biochar (CFS450) were collected, ground, and sieved to a uniform size of 0.9–1.2 mm. The ground biochar was washed several times with deionized water to remove impurities. Then, it was dried at 80 °C in an oven and sealed in a container for later use (Yao et al. 2011).

To make the modified biochar (MCFS450), the crayfish shell was soaked in the 3.0 M ZnCl_2 solution at a solid-liquid ratio of 1.0 g to 2.8 mL for 2 h. The modified biochar was produced with the same method mentioned above.

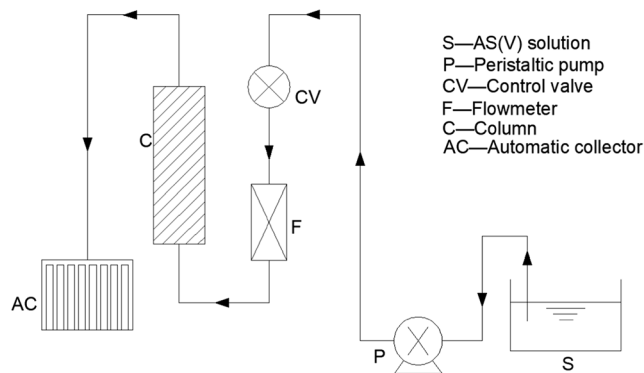


Fig. 1 Experimental setup of dynamic column adsorption

Characterizations

Element composition was determined by an Elemental Analyzer (Vario EL III, Elmentar, German). The surface morphology was acquired by scanning electron microscopy (JEM-6700F, Hitachi Limited, Japan). Specific surface areas were determined by a surface area analyzer (AsAP2020, micromeritics, USA) using both BET and N_2 adsorption methods. The presence of surface functional groups on the samples was verified by Fourier transform infrared spectroscopy (FTIR, Ascolet 6700, Thermo Ascolet, USA). Crystalline minerals on either pre- or post-sorption samples were detected by X-ray diffractometer (XRD, X’Pert Pro, PANalytical, the Netherlands).

Batch sorption of As(V)

About 0.1 g biochar was mixed with 50 mL $\text{Na}_3\text{AsO}_4 \cdot 12\text{H}_2\text{O}$ solution (40 mg/L As(V)) in a 50 mL centrifuge tube (Xu et al. 2012). Then, the centrifuge tube was shaken in a mechanical shaker (150 r/min) at 25 °C for 24 h. After the adsorption, 0.22- μm membrane filter was used to separate the biochar from the solution. As(V) adsorption amount q (mg/g) can be calculated as follows:

$$q = \frac{(C_0 - C_1)V}{m_0} \tag{1}$$

where C_0 is the initial concentration of As(V), C_1 is the equilibrium concentration of As(V) (mg/L), V is the volume of solution (L), and m_0 is the weight of biochar (g).

Table 1 Elemental composition of biochar

Biochar	C (%)	H (%)	N (%)	Zn (%)	As (%)
CFS450	47.63	0.3125	1.28	0.22	0.98
MCFS450	22.83	0.2175	1.26	22.83	1.97

Table 2 Specific surface area and pore structure of biochar

Biochar	BET-specific surface area (m ² /g)	Microporous specific surface area (m ² /g)	Pore volume (cm ³ /g)	Micropore volume (cm ³ /g)	Average pore size (nm)
CFS450	28.2989	8.9864	0.085266	0.004600	120.5219
MCFS450	134.1901	95.8200	0.105048	0.049688	31.3131

Effect of pH, reaction temperature, and coexisting anions

Under the conditions of different temperatures, pH, and coexisting ions, 0.1 g biochar was used to adsorb 50 mL 40 mg/L As(V) solution for 24 h. pH was adjusted by 1 M NaOH and HCl solutions (1 + 10). PO₄³⁻, HCO₃⁻, SO₄²⁻, and Cl⁻ were selected as coexisting anions, and the concentration of coexisting anions was set at 10 mg/L. Details of the three influencing factors are found in Figs. 6, 7, and 8.

Mathematical models

Pseudo-first-order, pseudo-second-order, and Elovich models were used to describe the sorption kinetic data. The governing equations of these models can be written as follows (Gola et al. 2017):

$$\text{Pseudo-first-order} : q_t = q_e(1 - e^{-k_1 t}) \quad (2)$$

$$\text{Pseudo-second-order} : q_t = \frac{k_2 q_e^2 t}{1 + k_2 q_e^2 t} \quad (3)$$

$$\text{Elovich} : qt = \frac{1}{\beta} \ln(\alpha\beta t + 1) \quad (4)$$

where q_t and q_e are the amounts of As(V) removed at time t and at equilibrium, respectively (mg/g); k_1 and k_2 are the pseudo-first-order and pseudo-second-order sorption rate constants (1/h), respectively; α is the initial sorption rate (mg/g); and β is the desorption constant (g/mg).

The Langmuir and Freundlich models were used to simulate the sorption isotherms. Their governing equations can be written as follows (Nguyen et al. 2017).

$$\text{Langmuir} : q_e = \frac{K S_{\max} C_e}{1 + K C_e} \quad (5)$$

$$\text{Freundlich} : q_e = K_f C_e^{1/n} \quad (6)$$

where K and K_f are the Langmuir bonding term related to interaction energies (L/mg) and the Freundlich affinity coefficient (mg⁽¹⁻ⁿ⁾Lⁿ/g), respectively, S_{\max} is the Langmuir maximum capacity (mg/kg), C_e is the equilibrium solution concentration (mg/L) of the sorbate, and n is the Freundlich linearity constant.

Column adsorption

The experimental setup is shown in Fig. 1. A certain amount of MCFS450 was loaded into a PVC column with a diameter of 15 mm and a height of 75 mm. As(V) solution was injected into the adsorption column from bottom to top at a certain flow rate. Effluent was collected by an automatic collector and flow rate was monitored and controlled by a control valve and a flowmeter.

Results and discussion

Biochar properties

The element analysis showed that CFS450 contained very little Zn, while MCFS450 had a large amount of Zn (Table 1). The arsenic content of MCFS450 was significantly higher than that of CFS450. High Zn content in the biochar can make its surface positively charged (Khan et al. 2011) and thus improve its adsorption capacity to anions (Bhatnagar et al. 2008).

Fig. 2 SEM image of **a** CFS450 and **b** MCFS450

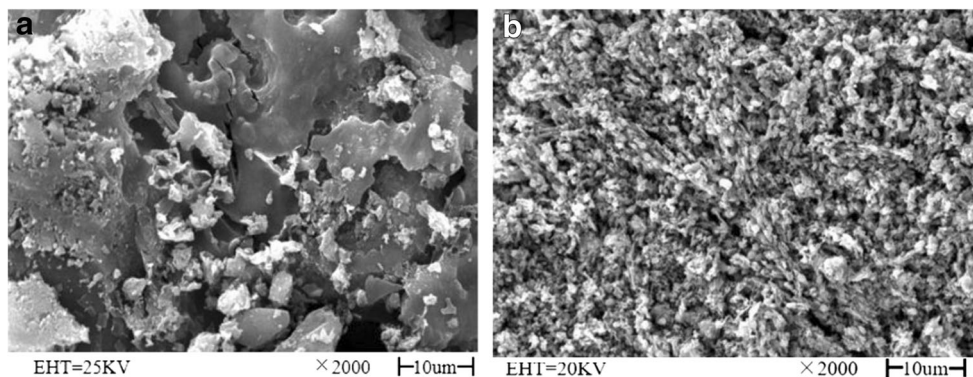
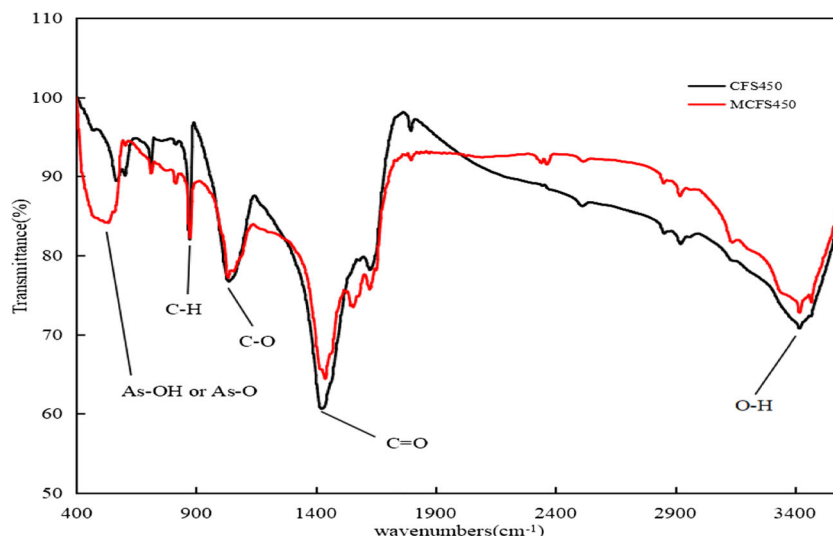


Fig. 3 FTIR spectra of the biochars



The specific surface areas analysis (Table 2) indicated that the BET-specific surface area and micropore surface area of MCFS450 increased significantly after modification. High specific surface area can improve the surface adsorption capacity of MCFS450.

SEM images showed that MCFS450 was looser and had more voids than CFS450 (Fig. 2). This is consistent with the BET-specific surface area measurement. Adsorption of As(V) on an adsorbent may be closely related to the pore structure, and well-developed pore structure may be more beneficial to the physical adsorption (Trakal et al. 2014).

As shown in Fig. 3, the biochar surface was rich in functional groups including C, H, and O elements (Zhang et al. 2016). The difference between CFS450 and MCFS450 was not significant. The wide and strong absorption peak at 3419/cm suggested the presence of -OH stretching vibrations (Cebi et al. 2017). The peak at 1417/cm was caused by C=O (Niazi et al. 2017). Liu et al. (2015) proved that both O-H and C=O groups were associated with the adsorption of As(V). Compared to CFS450, MCFS450 had a strong and broad absorption peak at 532/cm, which was related to the stretching vibrations of AsOH or AsO (Lata and Samadder 2016; Qian et al. 2013).

The XRD analysis (Fig. 4 and 5) showed that the diffraction peaks between the CFS450 and MCFS450 differed greatly. There was CaCO₃ crystal on CFS450, while the ZnO crystal was founded on MCFS450. After the modification, CaCO₃ crystal was converted into ZnCO₃ crystal and then ZnCO₃ was further decomposed into ZnO under high temperature conditions. The generated gas expanded the number of micropores on biochar and increased the BET-specific surface area and the micropore surface area, which is consistent with the data in Table 2.

Effects of pH, temperature, and coexisting anions

At pH = 1.48, the As(V) adsorption capacity of MCFS450 was 14.87 mg/g. As the pH increased, the adsorption capacity

decreased (Fig. 6). When the pH value increased, the surface of the biochar may change from being positively charged to negatively charged to reduce the adsorption capacity to anions (Garfield et al. 2014).

According to Fig. 7, as the temperature arose, the adsorption capacity increased, indicating that the adsorption process is an endothermic process.

Figure 8 shows that as Cl⁻, HCO₃⁻, SO₄²⁻, and PO₄³⁻ coexisted in the solution, the adsorption capacity decreased. The order of influence was PO₄³⁻ > SO₄²⁻ > HCO₃⁻ > Cl⁻. The main reasons are summarized as follows: (1) The adsorption of high-valent anions is greater than that of low-valent anions. (2) The properties of PO₄³⁻ and AsO₄³⁻ are similar, resulting in the two anions competing for active adsorption sites. (3) The hydrolysis of HCO₃⁻ increases the pH of the solution and thus has a stronger effect than Cl⁻.

Adsorption kinetics and isotherms

According to Fig. 9, As(V) sorption kinetics on MCFS450 can be divided into two stages: at the first few hours, the adsorption rate increased rapidly and then the rate gradually became stable. Pseudo-first-order, pseudo-second-order, and Elovich models were used to simulate the sorption kinetics data (Table 3). The adsorption process was best fitted by the pseudo-first-order model ($R^2 = 0.987$). More than 90% of the sorption capacity had been accomplished in the early 10 h. In consideration of the large specific surface area of the biochar samples, surface adsorption was the predominant force to control the sorption process in the initial stage. Beside the positively charged structure and ZnO nanoparticles, the electrostatic attraction was the vital factor to play a crucial part in the sequent adsorption stage.

Langmuir and Freundlich models were used to simulate the sorption isotherm data (Table 5). The best fitted model was the Langmuir model with the correlation coefficient of 0.976, while the correlation coefficient of Freundlich

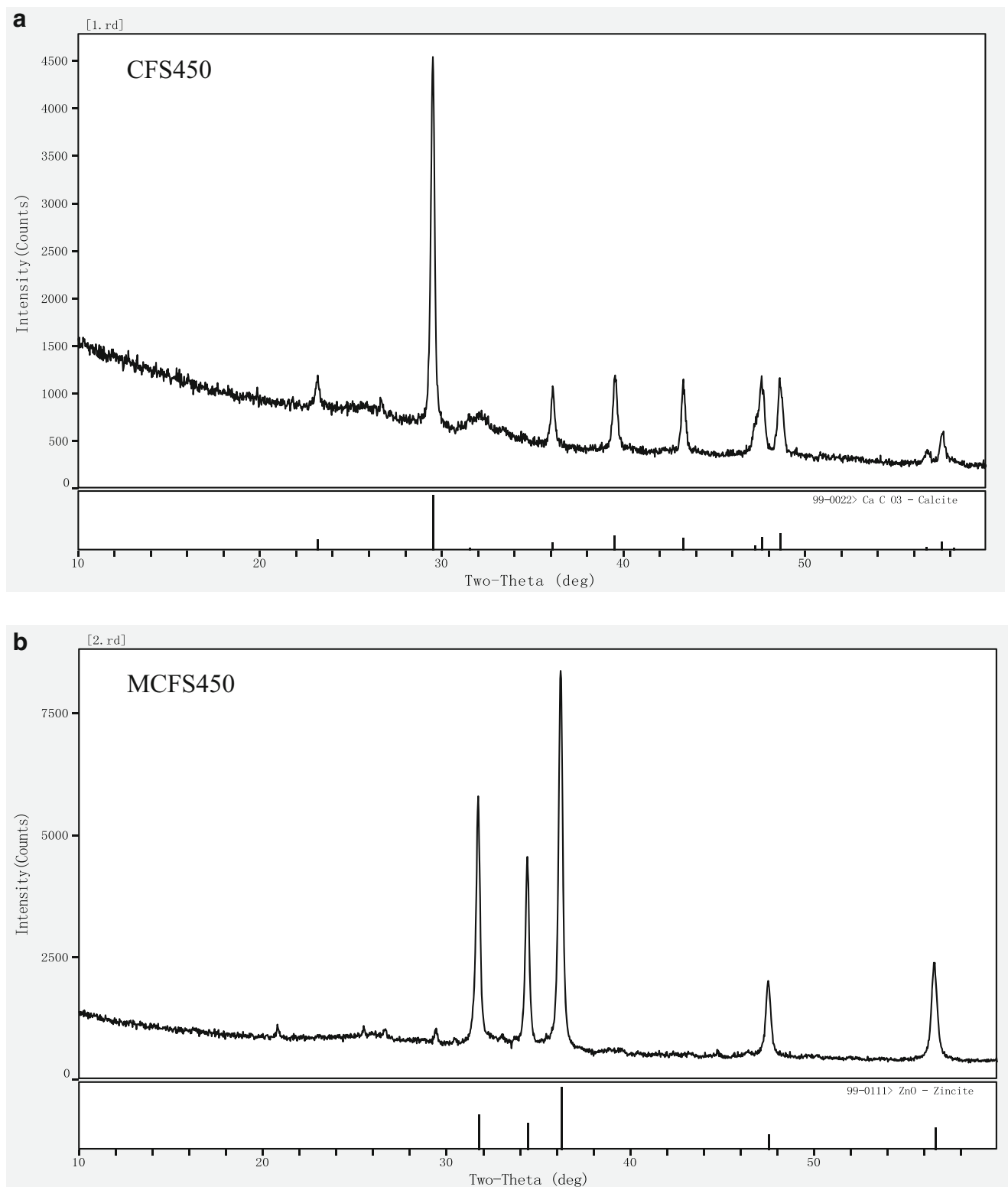
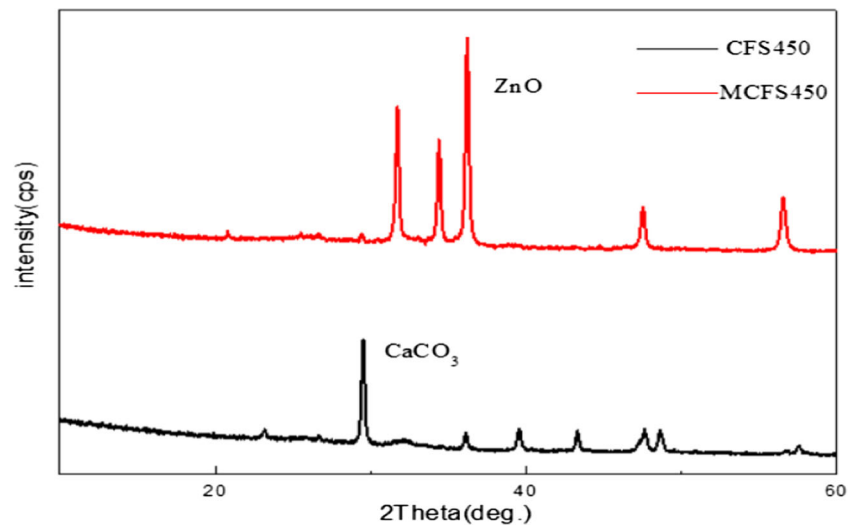


Fig. 4 XRD analysis of **a** CFS450 and **b** MCFS450

was 0.872. Based on Langmuir model, the maximum sorption capacity of MCFS450 to As(V) was 17.2 mg/g (Fig. 10). The better fitted of the Langmuir model indicates that the As(V) removal belonged to monolayer

sorption. In some sense, the monolayer sorption demonstrates that the considerable adsorption capacity of As(V) onto MCFS450 can be attributed to the high specific surface area.

Fig. 5 The analysis of phase identifying for the crystal on biochar surface



Adsorption mechanism

The batch experimental data suggest that the adsorption was mainly controlled by three mechanisms: physical adsorption, complexation reaction, and electrostatic adsorption. MCFS450 had a large specific surface area and rich pore structure, making it have a higher physical adsorption capacity. The FTIR spectra showed that arsenic had reacted with functional groups including O on the surface of biochar, and there existed stretching vibrations of AsOH or AsO. The presence of ZnO nanoparticles on the MCFS450 increased the zeta potential of the surface. Therefore, MCFS450 could adsorb AS(V) by electrostatic attraction.

Column study

The breakthrough time (t_b) of this work was defined as the time when the effluent concentration (C_t) reached 90%

of the influent value ($C_t/C_0 = 0.9$). Breakthrough curves were plotted-giving ratio of effluent and influent concentrations (C_t/C_0) and time (min) for varying operating conditions.

Effect of flow rate (Q_0)

Effect of Q_0 on the As(V) breakthrough curves (Fig. 11) was determined with the amount of biochar (M) of 2 g and influent concentration (C_0) of 40 mg/L. As the flow rate increased from 5 to 10 mL/min, the breakthrough time (t_b) decreased from 46.7 to 26.3 min. The results indicated that compared with the low flow rate, there might be a larger mass transfer coefficient at high flow rate, which made the adsorption column be saturated in a shorter time and the breakthrough time became shorter (Mai et al. 2018).

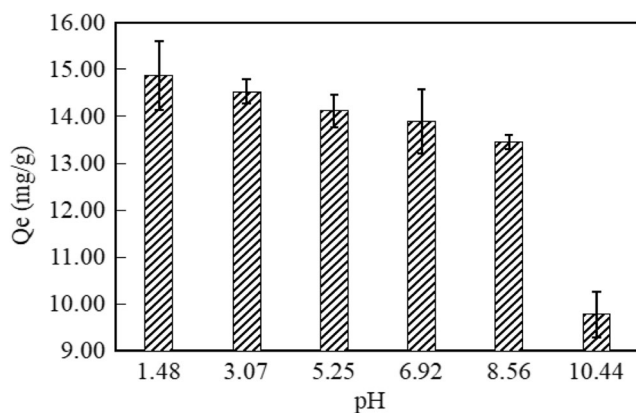


Fig. 6 Effect of pH on As(V) removal by MCFS450

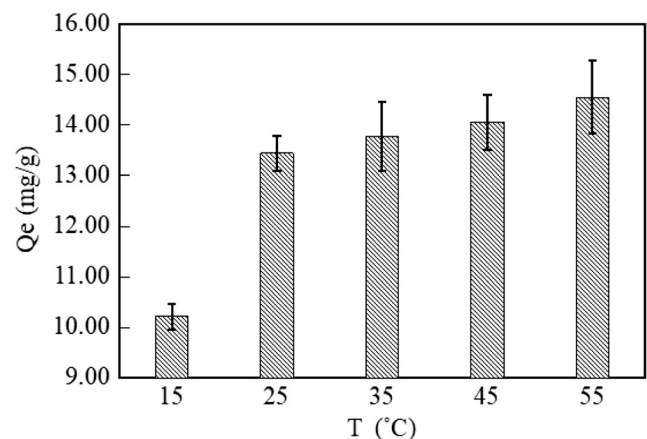


Fig. 7 Effect of temperature on As(V) removal by MCFS450

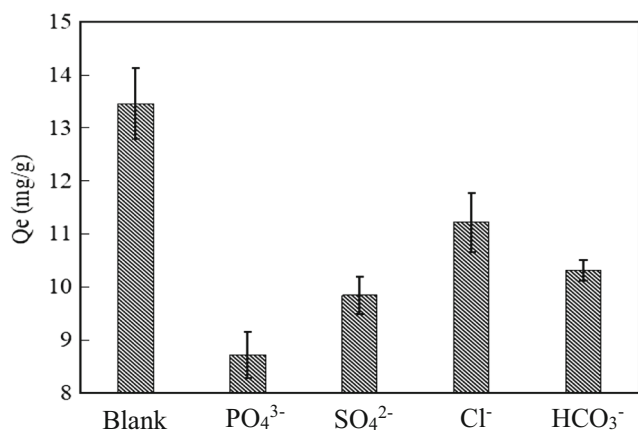


Fig. 8 Effect of coexisting anions on As(V) removal by MCFS450

Effect of initial concentration (C₀)

Effects of initial concentration on the breakthrough curves (Fig. 12) were conducted using 2 g biochar (*M*) at the flow rate of (*Q*₀) 5 mL/min. It is illustrated that the adsorption process reached saturation faster and the breakthrough time (*t*_b) decreased with increasing initial concentration (Table 4) (Olgun et al. 2013). When the initial concentration was high, the driving force of mass transfer was large, and the adsorption site of biochar was occupied by As(V) rapidly, so that the length of the adsorption zone decreased and the breakthrough time became shorter.

Effect of biochar quality (*M*)

Effects of biochar quality (*M*) on the breakthrough curves (Fig. 13) were conducted with influent concentration (*C*₀) of 40 mg/L and at the flow rate of (*Q*₀) 5 mL/min. As *M* increased, the adsorption zone and residence time increased correspondingly. In fact, it increased the length of the mass transfer belt so that the filter layer was less likely to be broken.

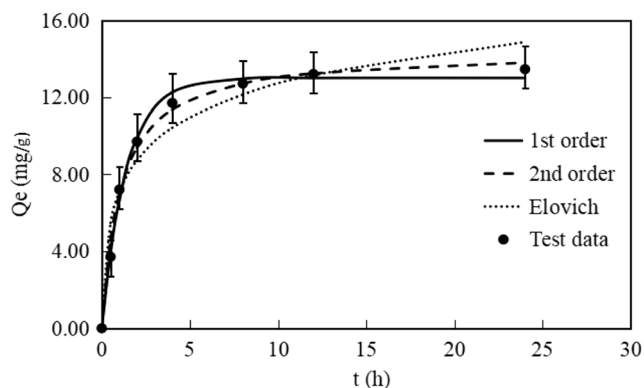


Fig. 9 Kinetics of As(V) adsorption onto MCFS450

Table 3 Best-fit model parameters of As(V) sorption onto MCFS450

Biochar	Model	Parameter 1	Parameter 2	R ²
MCFS450	Pseudo-first-order	<i>k</i> ₁ = 0.7131	<i>q</i> _e = 13.0 mg/g	0.987
	Pseudo-second-order	<i>k</i> ₂ = 0.0643	<i>q</i> _e = 14.4 mg/g	0.985
	Elovich	<i>α</i> = 39.592	<i>β</i> = 0.3995	0.898
	Langmuir	<i>K</i> = 0.17	<i>Q</i> _{max} = 17.2 mg/g	0.976
	Freundlich	<i>K</i> _f = 4.42	<i>n</i> = 0.304	0.872

Modeling of column adsorption

The equations of the Thomas (Muliwa et al. 2018), Yoon-Nelson (Yoon and Nelson 1984), and Adams-Bohart (Goel et al. 2005) models can be written as follows:

$$\text{Thomas : } \frac{C_t}{C_0} = \frac{1}{1 + \exp\left(\frac{M}{Q_0} \cdot K_T \cdot q_e - C_0 \cdot K_T \cdot t\right)} \quad (7)$$

$$\text{Yoon-Nelson : } \ln\left(\frac{C_t}{C_0} - C_t\right) = K_{YN} \cdot (t - \tau) \quad (8)$$

$$\text{Adams-Bohart : } t = \frac{N_0}{C_0 V} \cdot X - \ln\left(\frac{C_0}{C_t} - 1\right) \cdot \frac{1}{C_0 K_{AB}} \quad (9)$$

where *t* is the breakthrough time (min), *C*₀ is the influent concentration (mg/l), *C*_{*t*} is the concentration at breakthrough time (mg/l), *q*_e is the adsorptive capacity(mg/g), *M* is the mass of the bed (g), *Q*₀ is the flow rate (L/min), *K*_T is the Thomas rate constant (l/(mg min)), *τ* is time when *C*_{*t*}/*C*₀ = 0.5, *K*_{YN} is the Yoon-Nelson rate constant (/min), *X* is the bed depth of column (cm), *N*₀ is the adsorptive capacity of the adsorbent

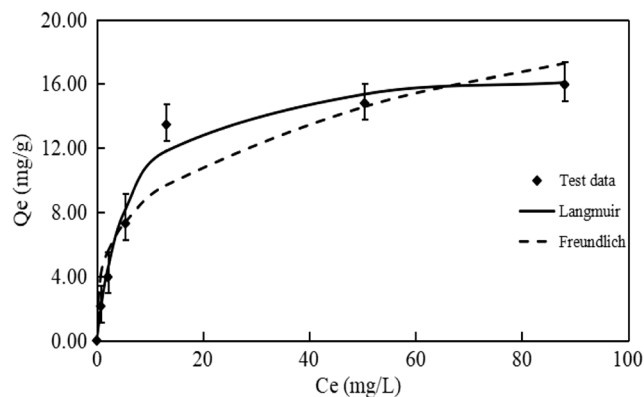
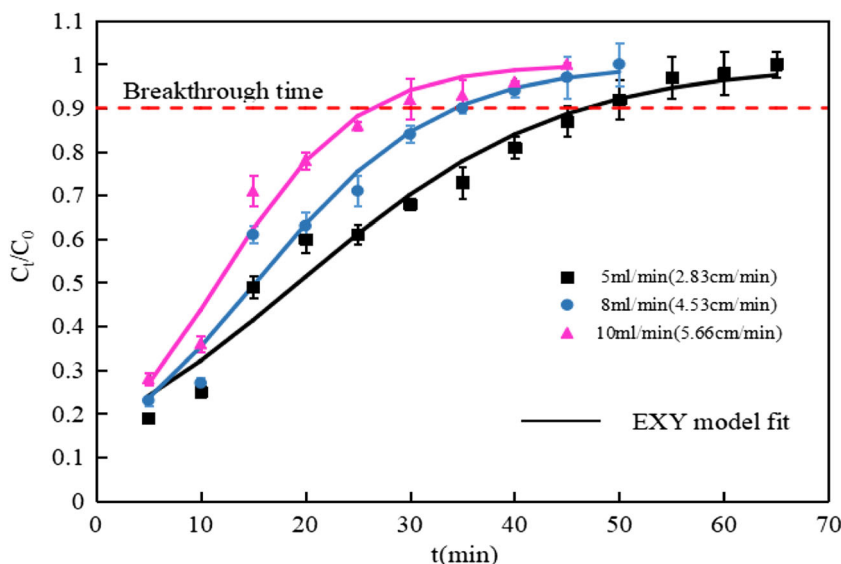


Fig. 10 Isotherm of As(V) adsorption onto MCFS450

Fig. 11 Effect of Q_0 on As(V) breakthrough curve



(mg adsorbed per liter of solution), V is the linear flow rate (cm/min), and K_{AB} is the Adams-Bohart rate constant (l/(mg min)).

The fitting results of the above three models were almost the same (Table 3). After rearrangement, the Eqs. (8) and (9) can be written as follows:

$$\text{Yoon-Nelson} : \frac{C_t}{C_0} = \frac{1}{1 + \exp(\tau \cdot K_Y - K_Y \cdot t)} \tag{10}$$

$$\text{Adams-Bohart} : \frac{C_t}{C_0} = \frac{1}{1 + \exp\left(\frac{X}{V} \cdot N_0 \cdot K_{AB} - C_0 \cdot K_{AB} \cdot t\right)} \tag{11}$$

Therefore, Eqs. (7), (10), and (11) can be expressed as a unified equation (EXY model):

$$\text{EXY model} : \frac{C_t}{C_0} = \frac{1}{1 + \exp(T - K_Y \cdot t)} \tag{12}$$

where t is the breakthrough time (min), C_0 is the influent concentration (mg/L), C_t is the concentration at breakthrough time (mg/L), T is a dimensionless constant, and K_Y is the EXY rate constant (/min).

Table 5 shows that the Thomas, Yoon-Nelson, and Adams-Bohart models are just the special forms of the EXY model. According to Table 4, EXY model ($R^2 = 0.97-0.99$) has a perfect fit for the breakthrough curve and can be used to predict the performance of continuous adsorption columns.

Fig. 12 Effect of initial concentration on As(V) breakthrough curve

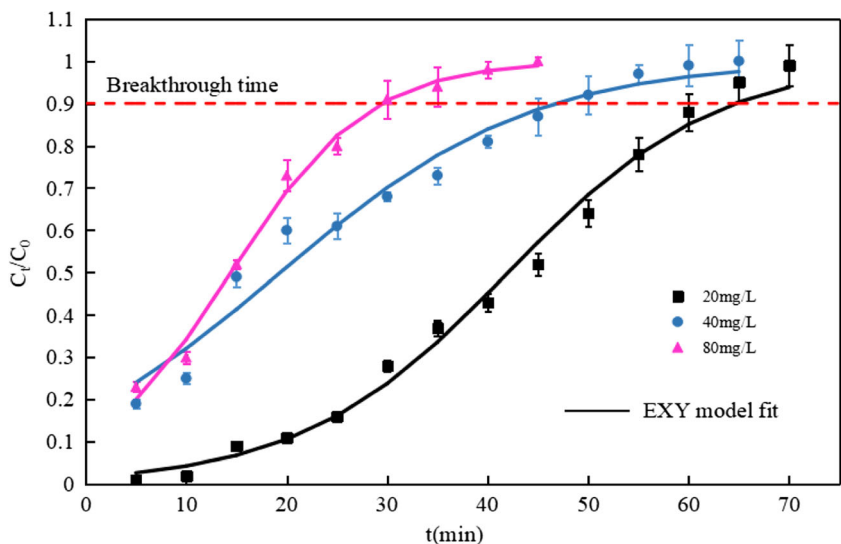
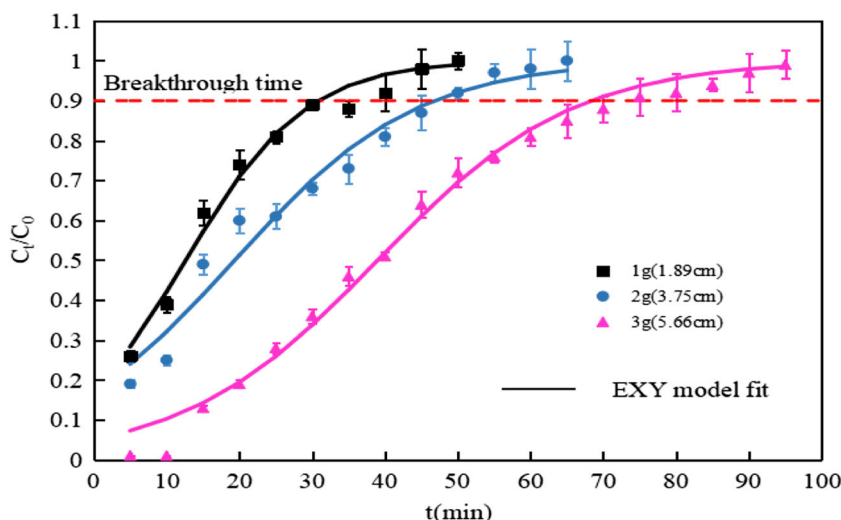


Table 4 Parameters of the Thomas, Adams-Bohart, Yoon-Nelson, and EXY models

Operation parameters				Thomas model			Yoon-Nelson model			Bohart-Adams model			EXY model		
C_0	Q	M	t_b	K_T	q_e	R^2	K_{YN}	τ	R^2	K_{AB}	N_0	R^2	T	K_Y	R^2
20	5	2	64.7	4.85	2.10	0.99	0.10	42.1	0.99	4.85	634.6	0.99	4.08	0.10	0.99
40	5	2	46.7	2.01	1.94	0.97	0.08	19.4	0.97	2.01	584.8	0.97	1.56	0.08	0.97
80	5	2	29.4	1.84	2.85	0.99	0.15	14.5	0.99	1.84	873.6	0.99	2.12	0.15	0.99
40	8	2	34.3	2.88	2.45	0.97	0.12	15.3	0.97	2.88	738.3	0.97	1.76	0.12	0.97
40	10	2	26.3	3.77	2.34	0.97	0.15	11.7	0.97	3.77	706.2	0.97	1.76	0.15	0.97
40	5	1	30.7	3.04	2.53	0.98	0.12	12.6	0.98	3.04	757.2	0.98	1.54	0.12	0.98
40	5	3	68.3	1.88	2.60	0.99	0.08	39.0	0.99	1.88	784.4	0.99	2.93	0.08	0.99

C_0 (mg/L), influent concentration; Q (L/min), flow rate; M (g), the mass of the bed; t_b (min), the time when the effluent concentration (C_t) reached 90% of the influent value ($C_t/C_0 = 0.9$); K_T ($\times 10^{-3}$ L/min \times mg), the Thomas rate constant; q_e (mg/g), the adsorptive capacity; K_{YN} (/min), the Yoon-Nelson rate constant; τ (min), the time when $C_t/C_0 = 0.5$; K_{AB} ($\times 10^{-3}$ L/(mg \times min)), the Adams-Bohart rate constant (l /(mg min)); N_0 (mg/L), the adsorptive capacity of the adsorbent; T , the dimensionless constant; K_Y (/min), the EXY rate constant

Fig. 13 Effect of biochar quality (M) on As(V) breakthrough curve



Conclusion

This work studied the removal of As(V) from aqueous solutions using crayfish shell biochar in batch and fixed bed column processes. After the modification by ZnCl₂, ZnO nanoparticles were generated on the surface of biochar, which improved its ability to absorb As(V). The pseudo-first-order model and the Langmuir model have the best fit for the experimental data. The Thomas, Yoon-Nelson, and Adams-Bohart models were used to describe the behavior of the

column adsorption process, and the three models could be expressed as a unified model (EXY model). The conclusion showed a high correlation (ranging from $R^2 = 0.97-0.99$) exhibited between experimental and predicted values using EXY model.

Acknowledgments The authors also thank the anonymous reviewers for their invaluable insight and helpful suggestions.

Funding information This work was partially supported by the Fundamental Research Funds for the Central Universities (No. 2042016kf0173) and the Wuhan Water Engineering & Technology Co. Ltd.

Table 5 Intrinsic connection of the models

EXY model (T, K_Y)	Thomas model	$T = K_T q_e M / Q$ $K_Y = C_0 K_T$
	Yoon-Nelson model	$T = \tau K_{YN}$ $K_Y = K_{YN}$
	Bohart-Adams model	$T = K_T N_0 X / V$ $K_Y = C_0 K_{AB}$

References

Atar N, Olgun A, Wang SB, Liu SM (2011) Adsorption of anionic dyes on boron industry waste in single and binary solutions using batch and fixed-bed systems. J Chem Eng Data 56:508–516

- Bhatnagar A, Ji M, Choi YH, Jung W, Lee SH, Kim SJ, Lee G, Suk H, Kim HS, Min B (2008) Removal of nitrate from water by adsorption onto zinc chloride treated activated carbon. *Sep Sci Technol* 43:886–907
- Cebi N, Yilmaz MT, Sagdic O (2017) A rapid ATR-FTIR spectroscopic method for detection of sibutramine adulteration in tea and coffee based on hierarchical cluster and principal component analyses. *Food Chem* 229:517–526
- Colak F, Olgun A, Atar N, Yazicioglu D (2013) Heavy metal resistances and biosorptive behaviors of *Paenibacillus polymyxa*: batch and column studies. *J Ind Eng Chem* 19:863–869
- Egodawatta LP, Macoustra GK, Ngo LK, Jolley DF (2018) As and Sb are more labile and toxic to water spinach (*Ipomoea aquatica*) in recently contaminated soils than historically co-contaminated soils. *Environ Sci Processes Impacts* 20:833–844
- Gao F, Xue Y, Deng P, Cheng X, Yang K (2015) Removal of aqueous ammonium by biochars derived from agricultural residuals at different pyrolysis temperatures. *Chem Speciat Bioavailab* 27:92–97
- Garfield LD, Dixon D, Nowotny P, Lotrich FE, Pollock BG, Kristjansson SD, Doré PM, Lenze EJ (2014) Effect of synthesis methods on magnetic Kans grass biochar for enhanced As(III, V) adsorption from aqueous solutions. *Biomass Bioenergy* 71:299–310
- Goeil J, Kadirvelu K, Rajagopal C, Kumar GV (2005) Removal of lead(II) by adsorption using treated granular activated carbon: batch and column studies. *J Hazard Mater* 125:211–220
- Gola D, Malik A, Namburath M, Ahammad SZ (2017) Removal of industrial dyes and heavy metals by *Beauveria bassiana*: FTIR, SEM, TEM and AFM investigations with Pb(II). *Environ Sci Pollut Res Int* 25:1–11
- Jaiswal V, Saxena S, Kaur I, Dubey P, Nand S, Naseem M, Sing SB, Srivastava PK, Barik SK (2018) Application of four novel fungal strains to remove arsenic from contaminated water in batch and column modes. *J Hazard Mater* 356:98–107
- Jin H, Capareda S, Chang Z, Gao J, Xu Y, Zhang J (2014) Biochar pyrolytically produced from municipal solid wastes for aqueous As(V) removal: adsorption property and its improvement with KOH activation. *Bioresour Technol* 169:622–629
- Khan MA, Ahn Y-T, Kumar M, Lee W, Min B, Kim G, Cho D-W, Park WB, Jeon B-H (2011) Adsorption studies for the removal of nitrate using modified lignite granular activated carbon. *Sep Sci Technol* 46:2575–2584
- Lata S, Samadder SR (2016) Removal of arsenic from water using nano adsorbents and challenges: a review. *J Environ Manag* 166:387–406
- Li ZZ, Imaizumi S, Katsumi T, Tang XW, Chen YM (2010) Comment on JHM 142 (2007) 1-53 'Arsenic removal from water-wastewater using adsorbents—a critical review' by D Mohan and CU Pittman Jr. *J Hazard Mater* 175:1116–1117
- Liu CH, Chuang YH, Chen TY, Tian Y, Li H, Wang MK, Zhang W (2015) Mechanism of arsenic adsorption on magnetite nanoparticles from water: thermodynamic and spectroscopic studies. *Environ Sci Technol* 49:7726–7734
- Mai TV, Chao HP, Trinh TV, Le TT, Lin CC, Hai NT (2018) Removal of ammonium from groundwater using NaOH-treated activated carbon derived from corn cob wastes: batch and column experiments. *J Clean Prod* 180:560–570
- Muliwa AM, Leswif TY, Maity A, Ochieng A, Onyango MS (2018) Fixed-bed operation for manganese removal from water using chitosan/bentonite/MnO composite beads. *Environ Sci Pollut Res* 1–15
- Naito S, Matsumoto E, Shindoh K, Nishimura T (2015) Effects of polishing, cooking, and storing on total arsenic and arsenic species concentrations in rice cultivated in Japan. *Food Chem* 168:294–301
- Nguyen TC, Loganathan P, Nguyen TV, Kandasamy J, Naidu R, Vigneswaran S (2017) Adsorptive removal of five heavy metals from water using blast furnace slag and fly ash. *Environ Sci Pollut Res Int* 1–9
- Niazi NK, Bibi I, Shahid M, Ok YS, Burton ED, Wang H, Shaheen SM, Rinklebe J, Lüttge A (2017) Arsenic removal by perilla leaf biochar in aqueous solutions and groundwater: an integrated spectroscopic and microscopic examination. *Environ Pollut* 232:31
- Olgun A, Atar N, Wang SB (2013) Batch and column studies of phosphate and nitrate adsorption on waste solids containing boron impurity. *Chem Eng J* 222:108–119
- Qian W, Zhao AZ, Xu RK (2013) Sorption of As(V) by aluminum-modified crop straw-derived biochars. *Water Air Soil Pollut* 224:1610
- Trakal L, Šigut R, Šillerová H, Faturiková D, Komárek M (2014) Copper removal from aqueous solution using biochar: effect of chemical activation. *Arab J Chem* 7:43–52
- Xia D, Tan F, Zhang C, Jiang X, Chen Z, Li H, Zheng Y, Li Q, Wang Y (2016) ZnCl₂-activated biochar from biogas residue facilitates aqueous As(III) removal. *Appl Surf Sci* 377:361–369
- Xu N, Zhang B, Tan G, Li J, Wang H (2015) Influence of biochar on sorption, leaching and dissipation of bisphenol A and 17 α -ethynylestradiol in soil. *Environ Sci Processes Impacts* 17:1722–1730
- Xue Y, Gao B, Yao Y, Inyang M, Zhang M, Zimmerman AR, Ro KS (2012) Hydrogen peroxide modification enhances the ability of biochar (hydrochar) produced from hydrothermal carbonization of peanut hull to remove aqueous heavy metals: batch and column tests. *Chem Eng J* 200-202:673–680
- Yao Y, Gao B, Inyang M, Zimmerman AR, Cao X, Pullammanappallil P, Yang L (2011) Biochar derived from anaerobically digested sugar beet tailings: characterization and phosphate removal potential. *Bioresour Technol* 102:6273–6278
- Yoon YH, Nelson JH (1984) Application of gas adsorption kinetics. I. A theoretical model for respirator cartridge service life. *Am Ind Hyg Assoc J* 45:517–524
- Zhang D, Luo Q, Gao B, Chiang SD, Woodward D, Huang Q (2016) Sorption of perfluorooctanoic acid, perfluorooctane sulfonate and perfluoroheptanoic acid on granular activated carbon. *Chemosphere* 144:2336–2342
- Zhang W, Zheng J, Zheng P, Tsang DC, Qiu R (2015) Sludge-derived biochar for arsenic(III) immobilization: effects of solution chemistry on sorption behavior. *J Environ Qual* 44:1119